Quantum Electronics **38** (7) 620 – 633 (2008)

INVITED PAPER

PACS numbers: 42.70.Qs; 42.81.Wg; 42.79.Dj
DOI: 10.1070/QE2008v038n07ABEH013828

Optical properties of Bragg fibres

A.S. Biryukov, D.V. Bogdanovich, D.A. Gaponov, A.D. Pryamikov

***Abstract*. The electrodynamic problem of propagation of light in a fibre with a cladding made of coaxial dielectric layers with alternating values of the refractive index is solved. The fibre core is a dielectric, in particular, air with the lowest permittivity in the fibre structure. A method is described for determining the structure of the multilayer cladding of a fibre having the minimal optical loss of the guided radiation for a particular mode. Losses in a fibre with a cladding with quasi-periodic layer thicknesses are calculated and the dispersion properties of the fibre are analysed. The analysis is performed for the lowest TE and TM modes and for the lowest hybrid mode.**

Keywords: *optical fibre, photonic crystal, total internal reflection, dispersion, optical losses.*

1. Introduction

In the last decade a new direction in fibre optics related to the investigation of microstructure optical fibres has appeared and is being rapidly developed. One of the variants of such fibres is the so-called Bragg fibres.

It is known that light propagates in usual fibres in an optically denser core due to total internal reflection from its boundary. Therefore, the fibre properties (dispersion, optical loss, nonlinear parameters) are determined by the properties of the core material. However, there also exist other mechanisms providing the localisation of light and its directional propagation, in particular, in a fibre with a hollow core. The latter is possible, for example, when the fibre cladding is made of the so-called photonic crystal, in particular, a multilayer dielectric mirror, which is well known in optics. The mirror properties of such claddings are determined by Fresnel reflection from many interfaces of a multilayer structure with alternating values of the permittivity and the subsequent constructive interference of reflected waves. Because reflection from multilayer dielectric mirrors formally resembles X-ray scattering in crystals and is described by the Brag condition, fibres with multilayer periodic claddings and a core made of an optically less dense material were called Bragg fibres (BFs) [1]. A specific feature of these fibres is that radiation only in some spectral ranges can propagate in the core of a fibre with the given layered cladding. And vice versa, there exist only certain structures of BFs in which light at the given wavelength can propagate with comparatively small losses. In other words, radiation is efficiently localised in the fibre core by no means at any thicknesses of the periodic structure of the cladding, even if they are comparable with the radiation wavelength. Therefore, no wonder that BFs in which directional radiation is determined by a mechanism different from total internal reflection have a number of properties that considerably differ from the properties of standard two-layer fibres. This mainly concerns the mode composition of radiation, dispersion, and optical losses. In particular, optical losses and nonlinearity in hollow BFs with the air core in the case of strong reflection of the guided light from the multilayer cladding can be in principle very low.

It is accepted that the first theoretical study of a dielectric Bragg waveguide in the visible and IR spectral ranges was performed in [1]. Only the lowest of the TE modes was analysed and it was pointed out that BFs are potentially efficient mode filters and, therefore, they can operate in the single-mode regime even at large core diameters. At the same time, optical losses in BFs were not calculated and only the general scheme was proposed, which can be used in principle to calculate them. Later [2], concrete and rather pessimistic data about losses in BFs were reported. The authors of [2] explained large losses in hollow BFs (more than 10^6 dB km^{-1}) by the impossibility to provide the high efficiency of radiation coupling into a fibre. Because of the absence of data on the fibre structure, the wavelength of guided radiation, and the mode type, it is impossible to verify the results obtained in [2].

In [3], the optical properties of a hybrid mode (the HE_{11} mode, according to the author) of a BF made entirely of silica were calculated. The author of [3] concluded based on his calculations that it is this mode that should have the highest Q factor, and to achieve optical losses smaller than 0.1 dB km^{-1}, it is sufficient to have eight layers in the cladding, which in this case had the refractive-index contrast in neighbouring layers equal to 0.022.

In [4], a model BF was studied which contained 100 dielectric layers of thickness 1 μm with alternating refractive indices $n_1 = 1.51$ and $n_2 = 1.49$ (the refractive index of the fibre core was $n_0 = n_1$ and the radius of the core cross section was varied from 2.5 to 3.25 μm). The main conclusions of paper [4] are that the TE modes should have the

A.S. Biryukov, D.V. Bogdanovich, D.A. Gaponov, A.D. Pryamikov Fiber Optics Research Center, Russian Academy of Sciences, ul. Vavilova 38, 119333 Moscow, Russia; e-mail: biriukov@fo.gpi.ru

Received 20 February 2008
Kvantovaya Elektronika **38** (7) 620 – 633 (2008)
Translated by M.N. Sapozhnikov

lowest optical losses in a glass BF, while the TM modes should have the highest losses (optical losses for hybrid modes are intermediate), which obviously contradicts results of [3].

In [5], the TE modes of a composite BF with a hollow core and a large refractive-index contrast in cladding layers $n_1 = 3$ and $n_2 = 1.5$ were analysed in the asymptotic approximation of large arguments of cylindrical functions (plane wave approximation). The layer thicknesses were set equal to 0.13 and 0.265 μm, respectively, and the core radius was 1 μm. The distributions of the longitudinal magnetic and azimuthal electric components of the lowest TE were found. It was pointed out that in the case of such a large refractive-index contrast in layers, the field amplitudes should decrease with increasing the radial coordinate so rapidly that the optical loss related to radiation fibre modes ~ 0.2 dB km^{-1} can be achieved by using only twenty pairs of structure layers.

Note that multilayer dielectric waveguides were studied earlier in the microwave range in the plane wave approximation in papers of Russian researchers [6–10]. The theory developed in [10] was applied to the optical range as well and, unlike previous papers, it was found that the EH_{11} mode should have the lowest losses.

The transfer matrix method described in [11] for analysis of Bragg reflectors of cylindrical walls is analogous to the known method for plane multilayer mirrors [12]. The method allows one to find the geometrical parameters of the structure most efficiently reflecting cylindrical waves. It is pointed out that the method can be used to analyse multilayer cylindrical waveguides; however, concrete results are absent.

The waveguiding possibilities of a hollow BF with the refractive indices $n_1 = 4.6$ and $n_2 = 1.59$ in a broad IR range (5–16 μm) were demonstrated in [13]. As a rule, dielectrics with considerably different permittivities also have different coefficients of thermal expansion. It is rather difficult to fabricate a multilayer structure from such dielectrics in the technological process including the drawing of fibres from preforms. In [13], fibres were fabricated by depositing the components of a coaxial structure in layers (polymer and tellurium layers) on the external surface of a silica capillary followed by the dissolving of the latter in hydrofluoric acid. The fabricated waveguide was not subjected to drawing and had, as a result, a comparatively large diameter of a hollow core, which was equal to the external diameter of the glass capillary (1.92 mm). It is obvious that this technology cannot be used to fabricate long waveguides. The investigations of this BF showed the presence of the transmission band between 8 and 11.5 μm, whose width was independent of the angle of incidence of radiation on the cladding, and also a comparatively small decrease in transmission even at a small radius of fibre bending (~ 1 cm).

Silica Bragg fibres were fabricated comparatively recently. In [14, 15], fibres with three pairs of coaxial glass layers and a glass core with the refractive index lower than those of cladding layers were studied. The length of fibres studied in [13–15] did not exceed, as a rule, ~ 1 m, so that experimental data on losses and other quantitative parameters of the fibres were absent.

Later [16], however, comparatively long (several metres) hollow BFs with a large permittivity contrast in layers were fabricated by using a chalcogenide glass As_2Se_2 with the refractive index of ~ 2.8 and a thermoelastic polymer with the refractive index of ~ 1.55, which had matching thermal properties. These fibres had different geometrical parameters (core diameter and thickness of a multilayer cladding) for different transmission ranges. In particular, BFs with the hollow core diameters 700–750 μm had the main transmission band in the wavelength region from 10 to 11 μm (the second transmission band was at ~ 5 μm). The optical losses at the CO_2 laser wavelength 10.6 μm were 0.95 dB m^{-1}, which is considerably smaller than optical losses in As_2Se_3 (~ 10 dB m^{-1}) and is many orders of magnitude smaller than optical losses in polymers.

After 2000, many papers devoted to theoretical and experimental studies of BFs were published (see, for example, [17–44]). However, in none of the papers the fibre structure was optimised in detail to achieve minimal optical losses. It is possible that for this reason the optical properties of BFs were estimated quite differently in different papers, both rather optimistically [3, 21] and, on the contrary, pessimistically (for example, [2]). In our opinion, it is not definitely clear so far which of the modes in hollow and glass BFs is fundamental [4, 42, 43]. This situation stimulated us to reconsider this problem as a whole and to analyse the properties of BFs based on somewhat different concepts.

2. The theory

2.1 Basic equations and their solutions

The mechanism of formation of guided radiation in BFs, which differs from that inherent in usual fibres, should result in the different formulation of the problem of analysing their properties. Instead of searching for the field distribution in a fibre with a preliminarily specified light-guiding structure, as is done for usual two-layer fibres and most of the theoretical studies of BFs, we will find, on the contrary, the structure of a fibre in which the field should not only satisfy the boundary conditions but also should be maximally localised in an optically less dense core.

We start, as usual, from Maxwell's equations, by representing them in the form of wave equations. We assume that light propagates in a dielectric medium with the magnetic susceptibility equal to unity everywhere and the permittivity ε is invariable in time and uniform in each of the layers of the fibre cladding (step radial profile of the distribution of ε). The time dependences of the electric $\boldsymbol{E}_0$ and magnetic $\boldsymbol{H}_0$ components of the field can be written in the form $\boldsymbol{E}_0 = \boldsymbol{E}\mathrm{e}^{-\mathrm{i}\omega t}$ and $\boldsymbol{H}_0 = \boldsymbol{H}\mathrm{e}^{-\mathrm{i}\omega t}$. Then, the vectors $\boldsymbol{E}$ and $\boldsymbol{H}$ in fibre cladding layers and core satisfy the wave equations

$$\left(\Delta + \frac{\omega^2\varepsilon}{c^2}\right)\left\{\begin{array}{c} E \\ H \end{array}\right\} = 0. \tag{1}$$

Equations (1) for the longitudinal field components E_z and H_z (denoted by Q) in the cylindrical coordinate system (r, φ, z) have the known form

$$\frac{1}{r}\frac{\partial}{\partial r}r\frac{\partial Q}{\partial r} + \frac{1}{r^2}\frac{\partial^2 Q}{\partial \varphi^2} + \frac{\partial^2 Q}{\partial z^2} + \frac{\omega^2\varepsilon}{c^2}Q = 0. \tag{2}$$

We assume that the cladding permittivity, which is uniform along z and φ, has only two values alternating in cladding layers. It is also assumed that each of the field

components depends on the longitudinal coordinate as $e^{i\beta z}$, where β is the phase propagation constant (the longitudinal component of the wave vector).

Under these assumptions, the solution of (2) has the form

$$Q = R(r)(G_1 \cos m\varphi + G_2 \sin m\varphi)e^{i\beta z}, \quad (3)$$

where m is the azimuthal parameter (for axially symmetric fibres, m is an integer, including zero); G_1 and G_2 are integration constants; and $R(r)$ is the radial part of the coordinate dependence of Q.

For the function $R(r)$, we obtain from (2) the Bessel equation

$$\frac{d^2R}{dr^2} + \frac{1}{r}\frac{dR}{dr} + \left(\kappa_j^2 - \frac{m^2}{r^2}\right)R = 0, \quad (4)$$

where $\kappa_j^2 = \varepsilon_j\omega^2/c^2 - \beta^2 = (2\pi n_j/\lambda)^2 - \beta^2$; κ_j are the transverse components of wave vectors in media with refractive indices $n_j = \sqrt{\varepsilon_j}$; and λ is the radiation wavelength in vacuum.

The solution of (4) in the general case is a combination of two linearly independent cylindrical functions. It is known that there exist several such combinations. Before choosing a particular solution of (4), note the following. We will assume that the fibre core has the refractive index n_0 and the refractive indices of alternating coaxial cladding layers are n_1 and n_2, and for definiteness $n_1 > n_2 > n_0$. Assume also that material losses in the fibre are absent ($\mathrm{Im}n_j = 0$; $j = 0, 1, 2$). In such a multilayer structure, numerous, both natural and quasi-natural waves can be excited. The natural waves are defined as slow waves with a discrete spectrum appearing due to total internal reflection and localised in optically dense cladding layers. The fields of quasi-natural, the so-called rapid waves are formed due to frustrated total internal reflection for cladding layers and are localised in the fibre core [10]. It is these radiation modes, which have the absolute maxima of the field components in the core but also possess some radiation losses, which we are interested in. The envelopes of radial distributions of the field components of such modes should be functions of r rapidly decreasing in magnitude. Only if this condition is fulfilled, the cladding properties of a mirror can be manifested. It is also clear the value of $\kappa_0^2 = (2\pi n_0/\lambda)^2 - \beta^2$ should be positive (κ_0 is the transverse wave number in the fibre core). Otherwise, the argument $\kappa_0 r$ of cylindrical functions in the solution of (4) proves to be imaginary, and the solution itself is represented only by one modified Bessel function of the first kind $I_m(\kappa_0 r)$, which monotonically increases with r and has no absolute extremum in the core [the second linearly independent cylindrical function $K_m(\kappa_0 r)$ of the imaginary argument has a singularity for $r = 0$ and should be excluded from consideration]. It follows from the above discussion that the main difference of a BF from a usual two-layer fibre is that the value of the effective mode refractive index $\bar{n} = \beta\lambda/2\pi$ in the usual fibre lies between the refractive indices of the fibre core and cladding, whereas this value for the BF should be smaller than the refractive index of the optically less dense core material, i.e. $\bar{n} < n_0$ (for a hollow BF, $\bar{n} < 1.0$).

It is easy to see that the condition $\kappa_0^2 > 0$ is fulfilled for purely imaginary values of the propagation constant β; however, they are of no interest because for such β there is no wave propagating along z.

It is clear that the complete absence of radial energy transfer would correspond to a structure representing an ideal cylindrical mirror. It is known that in this case a standing wave is formed along the radial coordinate, while the absence of energy transfer in it means that the time-averaged radial component S_r of the Poynting vector $\boldsymbol{S} \sim \mathrm{Re}[\boldsymbol{EH}^*]$ is zero. Recall that the electric energy in a standing wave completely transforms to the magnetic energy during a quarter of the period of electromagnetic oscillations and during the next quarter – vice versa, the magnetic energy transforms to the electric energy. In this case, the energy migrates from the antinodes of the electric field to the phase-shifted (by $\pi/2$) antinodes of the magnetic field and backward. The energy flux through the nodes of the electric and magnetic fields is identically zero (i.e. at any arbitrary instant of time). Each layer of the medium of optical thickness $\lambda/4$ from a node of the electric field to the nearest node of the magnetic field does not exchange energy with the environment. In a real, not ideally reflecting multilayer structure of a finite thickness (with a finite number of layers), a 'quasi-standing' wave is formed, which is a superposition of a standing wave and a wave travelling in the radial direction and determines optical losses. In other words, we define the 'quasi-standing' wave as a wave with the radial energy flux somewhat different from zero. In this respect, we can say only about a partial localisation of light in the BF core. Therefore, in the general case even in the absence of material losses in fibre layers, the propagation constant β is a complex quantity with the positive imaginary part. This imaginary part in turn should be a function of the radiation wavelength and the number of dielectric layers in the fibre cladding.

Each BF structure has the maximum reflectance of a cladding at a specific wavelength λ_0 of guided radiation. The shift of any side of λ_0, as a decrease in the number of layers in the cladding, leads, as will be shown below, to an increase in $\mathrm{Im}\beta$, increasing thereby optical losses {the real part of the exponent in the factor $\exp(i\beta z) = \exp[z(i\mathrm{Re}\beta - \mathrm{Im}\beta)]$ increases}. Below, it makes sense to analyse only BF structures with $\mathrm{Im}\beta \ll \mathrm{Re}\beta$; therefore, the condition $\bar{n} < n_0$ should be fulfilled for $\bar{n} \approx \lambda\mathrm{Re}\beta/2\pi$ with good accuracy.

According to the above consideration, we will write the solution of (4) in the form of a linear combination of linearly independent Bessel and Hankel functions of the first kind, which gives for Q

$$Q(r, \varphi, z) = (G_1 \cos m\varphi + G_2 \sin m\varphi) \times [C_1 J_m(\kappa r) + C_2 H_m^{(1)}(\kappa r)]e^{i\beta z}, \quad (5)$$

where C_1 and C_2 are two additional integration constants. For the time dependence of the field components that we use ($\sim e^{-i\omega t}$), the Hankel function $H_m^{(1)}$ determines a wave diverging from the symmetry axis. The superposition of the standing and travelling waves instead of the functions J_m and $H_m^{(1)}$ can be, of course, also described by other pairs of linearly independent cylindrical functions, in particular, $H_m^{(2)}$ and $H_m^{(1)}$ or, as in [1], by J_m and N_m (N_m is the Neumann function).

Taking into account that $H_m^{(1)}(\kappa r)$ has a singularity at $r = 0$, it is necessary to assume that $C_2 = 0$ for the cladding region in (5).

We further assume that the layered part of the cladding is surrounded by a very thick dielectric layer with the refractive index n_2 (or n_1). Based on physical considerations, the solution of (5) in this region should be represented only by the function $H_m^{(1)}$ (assuming that $C_1 = 0$). Indeed, here in the absence of interfaces between different media, there are no reflections of light and only diverging waves can exist. The latter statement is true if either the thickness of the external non-layered part of the cladding is infinite or the field intensity in it is small. In reality, the entire glass structure of a fibre is covered with a protective jacket made of polymers or other materials (in particular, metals). Therefore, the reflection of light from the additional glass-protective jacket interface should be taken into account in a number of cases [44].

The necessity of fulfilment of boundary conditions for any values of the azimuthal coordinate determines the constants G_1 and G_2 in (3) and (5), which are not arbitrary in this case. In other words, the solutions of (2) represent two variants of dependences on transverse coordinates (or two classes of waves) containing simultaneously either upper or lower trigonometric functions in braces in the expressions

$$E_z = [AJ_m(\kappa r) + BH_m^{(1)}(\kappa r)]\begin{Bmatrix}\cos m\varphi\\ \sin m\varphi\end{Bmatrix}e^{i\beta z},$$
$$H_z = [CJ_m(\kappa r) + DH_m^{(1)}(\kappa r)]\begin{Bmatrix}\sin m\varphi\\ \cos m\varphi\end{Bmatrix}e^{i\beta z}, \tag{6}$$

where A, B, C, and D are arbitrary constants.

By defining E_z and H_z in the form (6), we find with their help from Maxwell's equations the rest of the field components. Thus, the solution of equations (1) is represented by two sets of relations in accordance with the two possible variants of solutions (6):

$$E_z = [A_iJ_m(\kappa_j r) + B_iH_m^{(1)}(\kappa_j r)]\begin{Bmatrix}\cos m\varphi\\ \sin m\varphi\end{Bmatrix},$$
$$E_r = \frac{i\omega}{c\kappa_j^2}\left(\bar{n}\frac{\partial E_z}{\partial r} + \frac{1}{r}\frac{\partial H_z}{\partial\varphi}\right) = \frac{i\beta}{\kappa_j}\{[A_iJ'_m(\kappa_j r) + B_iH_m^{(1)'}(\kappa_j r)] + \frac{m}{\alpha\kappa_j r}[C_iJ_m(\kappa_j r) + D_iH_m^{(1)}(\kappa_j r)]\}\begin{Bmatrix}\cos m\varphi\\ \sin m\varphi\end{Bmatrix},$$
$$E_\varphi = \frac{i\omega}{c\kappa_j^2}\left(\frac{\bar{n}}{r}\frac{\partial E_z}{\partial\varphi} - \frac{\partial H_z}{\partial r}\right) = \frac{i\beta}{\kappa_j}\left\{\frac{m}{\kappa_j r}[A_iJ_m(\kappa_j r) + B_iH_m^{(1)}(\kappa_j r)] + \frac{1}{\alpha}[C_iJ'_m(\kappa_j r) + D_iH_m^{(1)'}(\kappa_j r)]\right\}\begin{Bmatrix}-\sin m\varphi\\ \cos m\varphi\end{Bmatrix}, \tag{7}$$
$$H_z = [C_iJ_m(\kappa_j r) + D_iH_m^{(1)}(\kappa_j r)]\begin{Bmatrix}\sin m\varphi\\ \cos m\varphi\end{Bmatrix},$$
$$H_r = \frac{i\omega}{c\kappa_j^2}\left(-\frac{\varepsilon_j}{r}\frac{\partial E_z}{\partial\varphi} + \bar{n}\frac{\partial H_z}{\partial r}\right) = \frac{i\beta}{\kappa_j}\left\{\frac{m\varepsilon_j}{\alpha\kappa_j r}[A_iJ_m(\kappa_j r) + B_iH_m^{(1)}(\kappa_j r)] + [C_iJ'_m(\kappa_j r) + D_iH_m^{(1)'}(\kappa_j r)]\right\}\begin{Bmatrix}\sin m\varphi\\ \cos m\varphi\end{Bmatrix},$$
$$H_\varphi = \frac{i\omega}{c\kappa_j^2}\left(\varepsilon_j\frac{\partial E_z}{\partial r} + \frac{\bar{n}}{r}\frac{\partial H_z}{\partial\varphi}\right) = \frac{i\beta}{\kappa_j}\left\{\frac{\varepsilon_j}{\alpha}[A_iJ'_m(\kappa_j r) + B_iH_m^{(1)'}(\kappa_j r)] + \frac{m}{\kappa_j r}[C_iJ_m(\kappa_j r) + D_iH_m^{(1)}(\kappa_j r)]\right\}\begin{Bmatrix}\cos m\varphi\\ -\sin m\varphi\end{Bmatrix},$$

where the subscript $j = 0, 1, 2$ is in accordance with the definition of k_j and n_j; $\alpha = \pm\beta c/\omega = \pm\bar{n}$; and the common factor for all field components is omitted. The subscript i of integration constants indicates that the corresponding solution belongs to the ith layer so that $r_{i-1} \leqslant r \leqslant r_i$, where r_i are coordinates of the interfaces between layers with different refractive indices, $i = 1, 2, \ldots, N$; N is the number of interfaces equal to the doubled number of layers with the high refractive index n_1, if the non-layered part of the cladding has the refractive index n_2; when this part has the refractive index n_1, N is larger by unity; $r \leqslant r_1$ corresponds to the core region. The prime at cylindrical functions means differentiation with respect to the argument. Solutions (7) are classified so that $\alpha = \bar{n}$ and $-\alpha = -\bar{n}$ correspond to the group with upper and lower, respectively, trigonometric functions in braces at the right.

The boundary conditions to which the solutions of the electrodynamic problem should satisfy require the continuity of the filed components (E_z, E_φ, H_z, H_φ) tangential to medium interfaces. It follows from (7) that in the general case ($m \neq 0$) these boundary conditions have the form

$$A_{l-1}J_m(x_{jl}) + B_{l-1}H_m^{(1)}(x_{jl}) = A_lJ_m(x_{pl}) + B_lH_m^{(1)}(x_{pl}),$$
$$\frac{m}{x_{jl}^2}[A_{l-1}J_m(x_{jl}) + B_{l-1}H_m^{(1)}(x_{jl})] + \frac{1}{\alpha x_{jl}}[C_{l-1}J'_m(x_{jl}) + D_{l-1}H_m^{(1)'}(x_{jl})] = \frac{m}{x_{pl}^2}[A_lJ_m(x_{pl}) + B_lH_m^{(1)}(x_{pl})] + \frac{1}{\alpha x_{pl}}[C_lJ'_m(x_{pl}) + D_lH_m^{(1)'}(x_{pl})],$$
$$C_{l-1}J_m(x_{jl}) + D_{l-1}H_m^{(1)}(x_{jl}) = C_lJ_m(x_{pl}) + D_lH_m^{(1)}(x_{pl}), \tag{8}$$
$$\frac{n_j^2}{\alpha x_{jl}}[A_{l-1}J'_m(x_{jl}) + B_{l-1}H_m^{(1)'}(x_{jl})] + \frac{m}{x_{jl}^2}[C_{l-1}J_m(x_{jl}) + D_{l-1}H_m^{(1)}(x_{jl})] = \frac{n_p^2}{\alpha x_{pl}}[A_lJ'_m(x_{pl}) + B_lH_m^{(1)'}(x_{pl})] + \frac{m}{x_{pl}^2}[C_lJ_m(x_{pl}) + D_lH_m^{(1)}(x_{pl})],$$

where $x_{jl} = \kappa_j r_l$; $x_{pl} = \kappa_p r_l$; the subscripts j and p correspond to two media separated by a cylindrical interface of radius r_l. In this case, the inmost interface has the radius r_l, so that $\kappa_j = \kappa_0$ and $\kappa_p = \kappa_1$ in it. Then, for $l = 2$, $\kappa_j = \kappa_1, \kappa_p = \kappa_2$, and for $l > 2$ the values κ_j and κ_p alternate.

2.2 Dispersion equations

Boundary conditions (8) are a system of $4N$ linear homogeneous algebraic equations for $4N$ integration constants $A_0, A_1, \ldots, A_{N-1}$; $B_1, B_2, \ldots, B_N$; $C_0, C_1, \ldots, C_{N-1}$; $D_1, D_2, \ldots, D_N$ (recall that $B_0 = D_0 = 0$ in the fibre core and $A_N = C_N = 0$ behind the layered structure). The nontrivial solution of this system exists if only its determinant is zero. The zero determinant represents a nonlinear dispersion equation determining the dependence of β on ω (or λ) for

the known fibre geometry (the known coordinates r_l) or, vice versa, the equation relating the propagation constant β with the structure geometry for fixed λ. Let us find this dispersion equation.

The calculation of the $4N \times 4N$ determinant for large values of N is quite time-consuming. However, in our case the calculation is simplified and is reduced to operations with quadratic 4×4 matrices. Indeed, boundary conditions (8) can be written in the matrix form

$$\begin{pmatrix} A_l \\ B_l \\ C_l \\ D_l \end{pmatrix} = M(r_l) \begin{pmatrix} A_{l-1} \\ B_{l-1} \\ C_{l-1} \\ D_{l-1} \end{pmatrix}, \tag{9}$$

where

$$M(r_l) = -\frac{i\pi x_{pl}}{2}(m_{ks}) \tag{10}$$

is the 4×4 matrix; k is the line number; and s is the column number. By using (8), it is easy to show that matrix elements in (10) are

$$m_{11} = J_m(x_{jl})H_m^{(1)'}(x_{pl}) - \frac{\varepsilon_j x_{pl}}{\varepsilon_p x_{jl}} J'_m(x_{jl})H_m^{(1)}(x_{pl}),$$

$$m_{12} = H_m^{(1)}(x_{jl})H_m^{(1)'}(x_{pl}) - \frac{\varepsilon_j x_{pl}}{\varepsilon_p x_{jl}} H_m^{(1)'}(x_{jl})H_m^{(1)}(x_{pl}),$$

$$m_{13} = \frac{\alpha m}{\varepsilon_p}\left(\frac{1}{x_{pl}} - \frac{1}{x_{jl}}\frac{x_{pl}}{x_{jl}}\right) J_m(x_{jl})H_m^{(1)}(x_{pl}),$$

$$m_{14} = m_{13}H_m^{(1)}(x_{jl})/J_m(x_{jl}),$$

$$m_{21} = \frac{\varepsilon_j x_{pl}}{\varepsilon_p x_{jl}} J'_m(x_{jl})J_m(x_{pl}) - J_m(x_{jl})J'_m(x_{pl}),$$

$$m_{22} = \frac{\varepsilon_j x_{pl}}{\varepsilon_p x_{jl}} H_m^{(1)'}(x_{jl})J_m(x_{pl}) - H_m^{(1)}(x_{jl})J'_m(x_{pl}),$$

$$m_{23} = -m_{13}J_m(x_{pl})/H_m^{(1)}(x_{pl}), m_{24} = -m_{14}J_m(x_{pl})/H_m^{(1)}(x_{pl}),$$

$$m_{31} = m_{13}\varepsilon_p, \quad m_{32} = m_{14}\varepsilon_p, \tag{11}$$

$$m_{33} = J_m(x_{jl})H_m^{(1)'}(x_{pl}) - \frac{x_{pl}}{x_{jl}} J'_m(x_{jl})H_m^{(1)}(x_{pl}),$$

$$m_{34} = H_m^{(1)}(x_{jl})H_m^{(1)'}(x_{pl}) - \frac{x_{pl}}{x_{jl}} H_m^{(1)'}(x_{jl})H_m^{(1)}(x_{pl}),$$

$$m_{41} = m_{23}\varepsilon_p, \quad m_{42} = m_{24}\varepsilon_p,$$

$$m_{43} = \frac{x_{pl}}{x_{jl}} J'_m(x_{jl})J_m(x_{pl}) - J_m(x_{jl})J'_m(x_{pl}),$$

$$m_{44} = \frac{x_{pl}}{x_{jl}} H_m^{(1)'}(x_{jl})J_m(x_{pl}) - H_m^{(1)}(x_{jl})J'_m(x_{pl}).$$

The elements of the matrix $M(r_l)$ are also presented in [1]. However, the matrix elements presented in [1] for $m \neq 0$ are incorrect, and we present here correct expressions.

One can see that transformation (9) of the field components is performed at each of the interfaces of the layered structure. By starting from the fibre core and performing these transformations the required number of times, we obtain

$$\begin{pmatrix} A_l \\ B_l \\ C_l \\ D_l \end{pmatrix} = M \begin{pmatrix} A_0 \\ 0 \\ C_0 \\ 0 \end{pmatrix} \tag{12}$$

for an arbitrary lth layer, where M is determined by the product of cofactors of type (10) and is also a 4×4 matrix $[M = \prod_1^l M(r_i)]$.

For $l = N$, matrix relation (12) is equivalent to a system of four linear homogeneous algebraic equations for constants A_0, C_0, B_N, and D_N. Their nontrivial solution exists only under the condition

$$\bar{m}_{11}\bar{m}_{33} - \bar{m}_{31}\bar{m}_{13} = 0, \tag{13}$$

where $\bar{m}_{ks}$ are the elements of the matrix M in (12) for $l = N$.

Obtained dispersion equation (13) is the required one. It satisfies the general boundary conditions and is valid for any geometry of a layered cladding and all the modes, both eigenmodes (cladding modes) and radiation modes (core modes).

Our problem now is to select from a set of solutions (7) satisfying general conditions (8) the solutions for which the cladding has the maximum reflection at a wavelength of λ_0.

We begin with the analysis of the simplest TM- and TE-mode families. These symmetric modes in (6)–(8), (11) correspond to $m = 0$, and only three components among a total set of field components (7) are nonzero. In particular, we have for the TM modes (upper trigonometric functions)

$$E_z = [A_i J_0(\kappa_j r) + B_i H_0^{(1)}(\kappa_j r)],$$

$$H_\varphi = -\frac{i\varepsilon_j \omega}{c\kappa_j}[A_i J_1(\kappa_j r) + B_i H_1^{(1)}(\kappa_j r)], \tag{14}$$

$$E_r = \frac{\bar{n}}{\varepsilon_j} H_\varphi,$$

and for the TE modes (lower trigonometric functions),

$$H_z = [C_i J_0(\kappa_j r) + D_i H_0^{(1)}(\kappa_j r)],$$

$$E_\varphi = \frac{i\omega}{c\kappa_j}[C_i J_1(\kappa_j r) + D_i H_1^{(1)}(\kappa_j r)], \tag{15}$$

$$H_r = -\bar{n}E_\varphi.$$

The boundary conditions for these modes also have a simpler form than (8)

$$A_{l-1}J_0(x_{jl}) + B_{l-1}H_0^{(1)}(x_{jl}) = A_l J_0(x_{pl}) + B_l H_0^{(1)}(x_{pl}),$$

$$\frac{\varepsilon_j}{x_{jl}}[A_{l-1}J_1(x_{jl}) + B_{l-1}H_1^{(1)}(x_{jl})] \tag{16}$$

$$= \frac{\varepsilon_p}{x_{pl}}[A_l J_1(x_{pl}) + B_l H_1^{(1)}(x_{pl})]$$

for the TM modes and

$$C_{l-1}J_0(x_{jl}) + D_{l-1}H_0^{(1)}(x_{jl}) = C_lJ_0(x_{pl}) + D_lH_0^{(1)}(x_{pl}),$$

$$\frac{1}{x_{jl}}[C_{l-1}J_1(x_{jl}) + D_{l-1}H_1\,(1)(x_{jl})] \tag{17}$$

$$= \frac{1}{x_{pl}}[C_lJ_1(x_{pl}) + D_lH_1^{(1)}(x_{pl})]$$

for the TE modes. Unlike (8), conditions (16) and (17) are the systems of $2N$ linear homogeneous algebraic equations for $2N$ constants $A_0,\ A_1, ..., A_{N-1}, B_1, ..., B_N$ or $C_0, C_1, ..., C_{N-1}, D_1, ..., D_N$ respectively.

The matrix $M(r_l)$ for the TM modes in (9) and (10) is the 2×2 matrix of the form

$$M(r_l) = -\frac{i\pi x_{pl}}{2}\begin{pmatrix} m_{11} & m_{12} \\ m_{21} & m_{22} \end{pmatrix}, \tag{18}$$

where the matrix elements m_{ks} have the form

$$m_{11} = \frac{\varepsilon_j x_{pl}}{\varepsilon_p x_{jl}} J_1(x_{jl})H_0^{(1)}(x_{pl}) - J_0(x_{jl})H_1^{(1)}(x_{pl}),$$

$$m_{12} = \frac{\varepsilon_j x_{pl}}{\varepsilon_p x_{jl}} H_1^{(1)}(x_{jl})H_0^{(1)}(x_{pl}) - H_0^{(1)}(x_{jl})H_1^{(1)}(x_{pl}), \tag{19}$$

$$m_{21} = J_0(x_{jl})J_1(x_{pl}) - \frac{\varepsilon_j x_{pl}}{\varepsilon_p x_{jl}} J_1(x_{jl})J_0(x_{pl}),$$

$$m_{22} = H_0^{(1)}(x_{jl})J_1(x_{pl}) - \frac{\varepsilon_j x_{pl}}{\varepsilon_p x_{jl}} H_1^{(1)}(x_{jl})J_0(x_{pl}).$$

Instead of (13), the dispersion equation takes the form

$$\bar{m}_{11} = 0, \tag{20}$$

where m_{11} is the element of the product matrix for factors of type (18).

For the TE modes, we obtain the same equations as (18)–(20); however, the ratio $\varepsilon_j/\varepsilon_p$ in expressions for the elements of the matrix $M(r_l)$ in (18) and (19) should be replaced by unity.

2.3 Optimisation of a multilayer BF structure

Note first that the Floquet–Bloch theorem in the cylindrical geometry, which is used, as rule, to analyse periodic structures, can be applied only in the asymptotic approximation [5]. The field components in the rectangular geometry are determined by the combinations of trigonometric functions with the invariable spatial period. Therefore, such a periodic structure can be described as a whole by using the Floquet–Bloch theorem. However, in the cylindrical geometry the field is represented by cylindrical functions with a period depending on the radial coordinate. Therefore, the thicknesses of layers of a multilayer BF cladding with alternating values of the refractive index should be the functions of this coordinate. In the general case the structure is quasi-periodic and only at large arguments of the functions the thicknesses of layers become asymptotically almost equal in each of the two their sequences. This specific feature of the cylindrical geometry should be taken into account in the rigorous consideration of this problem.

In the absence of material losses, optical losses in a fibre (due to radiation modes) and the degree of light localisation in the fibre core are determined by the radial component of the Poynting vector S_r. Therefore, the minimisation of S_r is the most natural way for obtaining the optimal geometry of a multilayer cladding. It is possible, for example, to require the maximum reflection of light from each of the layer interfaces. This method assumes the determination of total reflection (transmission) both in all previous (with respect to the symmetry axis) and all structure layers behind this interface. This method for calculating reflection and transmission in a multilayer coaxial structure is described in most detail probably in [45]; however, the optimisation of the structure geometry for obtaining maximum reflection was not discussed in this paper (see also [11]). In addition, it is clear that minimal optical losses can be also found by minimising the radial energy flux propagating behind the layered cladding for $r > r_N$ and explicitly determining radiation losses.

It seems that the two above-mentioned methods for minimising S_r are equivalent; however, we will not prove it, but simply will use the second method.

It was shown in papers [1, 4, 21, 27, 29, 30] that an important property of BFs is that they can be used as efficient mode filters and the TE_{01} mode in hollow BFs should have the highest Q factor. The latter is confirmed by the results of our calculations presented below. Therefore, when we are dealing with the optimisation of the multilayer structure of hollow BFs, it is reasonable to optimise it only for the lowest of the TE modes. The rest of the modes in this optimised BF should have considerably higher losses.

Let us write the expression for the time-averaged radial component of the energy flux vector $S_r = \mathrm{Re}(E_\varphi H_z^\bullet/2)$ for the TE modes on the last interface r_N of the layered cladding. This expression follows from (15), (17)–(19) and has the form

$$S_r(r_N) = -\frac{r_N\omega C_0^2}{2c}\left|\frac{\bar{m}_{21}}{x_N}\right|^2 \mathrm{Im}\{H_1^{(1)}(x_N)[x_NH_0^{(1)}(x_N)]^\bullet\}, \tag{21}$$

where $\bar{m}_{21}$ is the element of the product matrix for factors of type (18); $x_N = r_N\kappa_2$ for even N and $r_N\kappa_1$ for odd N. Because $S_r(r_N)$ is the function of coordinates of all layer interfaces, the optimisation of the cladding structure for obtaining the minimum radial energy flux is equivalent to the determination of the minimum of the right-hand side of (21) over N variables $r_1, r_2, ..., r_N$. It is possible to do it in a standard way by setting equal to zero all the first-order partial derivatives from (21) with respect to r_i (the necessary but not sufficient condition for the existence of the multidimensional extremum of the function). The system of homogeneous nonlinear equations for $r_1, r_2, ..., r_N, \beta$ obtained in this way should be closed with dispersion equation (20). The solution of such a system of equations for high enough N is, as a rule, a challenging independent problem.

We preferred another method and found the minimum of S_r with the help of the so-called genetic algorithm (see, for example, [46]), which is based on a direct analogy of the optimisation process with selection processes occurring in nature. The genetic algorithm operates by the 'populations' of potential solutions, by applying the survival principle to them and taking part in the formation of the 'descendants' of the most adapted solutions. The adaptability of each of the potential solutions is determined by the value of its target function [in or case, (21), (20)] estimating the difference of this solution from the required result. The higher the

adaptability of the solution, the higher probability that the useful features of the descendants obtained with the help of this solution and determining the adaptability will be manifested greater. 'The vector of variables' in the genetic algorithm plays the same role as a genotype in biology. The algorithm does not require the knowledge of the relief of a multidimensional surface on which an extremum is sought, it can come from local extrema, can be simply realised, does not require large computational resources and has been already tested by solving many problems (see details in [46]).

Thus, the optimal geometry of a BF is determined in the following way. The radius of the fibre core r_1 and the values of n_0, n_1, n_2, and N are assumed known for the specified wavelength λ_0 of guided radiation in the fibre. By using the genetic algorithm, the minimum of function (21) of variables $r_2, r_3, ..., r_N, \beta$ is sought when equation (20) is valid (optimisation of the BF to the TE mode). To each value of β, its own optimal geometry of the layered structure of the cladding corresponds, and therefore the propagation constant is included to the list of variables to be optimised. The solution of the problem should be the choice of the values of $r_2, r_3, ..., r_N, \mathrm{Re}\beta, \mathrm{Im}\beta$, which, on the one hand, would provide the absolute minimum of function (21) and, on the other, satisfy equation (20). In this case, because Eqn (20) for an arbitrary geometry $(r_2, r_3, ..., r_N)$ has a set of roots β, the root with the smallest possible value of $\mathrm{Im}\beta$ corresponds to the lowest TE_{01} mode of a hollow fibre. Note also that the genetic algorithm operates the better, the smaller the region of changing the variables of the function being optimised. In other words, both the initial values of coordinates $r_2, r_3, ..., r_N$ and $\mathrm{Re}\beta$ should be closer as possible to their real values.

The condition $\mathrm{Im}\beta = 0$ corresponds, as mentioned above, to the presence of a standing wave along the cross-section radius, when the time-averaged radial energy flux is zero for all values of r, which is possible only for a cladding consisting of the infinite number of alternating layers. To find the approximate parameters of the structure of a multilayer BF with a finite number of cladding layers under the condition $\mathrm{Im}\beta \ll \mathrm{Re}\beta$, when the radial energy flux is generally speaking nowhere equal to zero, we will assume, nevertheless, that $S_r = 0$ at all the nodes tangential to the interfaces of the field component layers. This means that we assume that the cladding of a real fibre consists of the infinite number of layers. We place the layer interfaces at the same nodes. The latter is achieved by solving the system of coupled equations following from (15) for the case of TE modes:

$$
\begin{aligned}
&E_{\varphi 1} = \frac{\mathrm{i}\omega}{c\kappa_0} C_0 J_1(\kappa_0 r_1) = 0,\\
&H_{z2} = C_1 J_0(\kappa_1 r_2) + D_1 H_0^{(1)}(\kappa_1 r_2) = 0,\\
&E_{\varphi 3} = \frac{\mathrm{i}\omega}{c\kappa_2}[C_2 J_1(\kappa_2 r_3) + D_2 H_1^{(1)}(\kappa_2 r_3)] = 0,\\
&H_{z4} = C_3 J_0(\kappa_1 r_4) + D_3 H_0^{(1)}(\kappa_1 r_4) = 0, \qquad (22)\\
&\ldots\ldots\ldots\ldots\ldots\ldots\ldots\ldots\ldots\ldots\ldots\ldots\ldots\ldots\ldots\ldots\\
&E_{\varphi(N-1)} = \frac{\mathrm{i}\omega}{c\kappa_2}[C_{N-2} J_1(\kappa_2 r_{N-1}) + D_{N-2} H_1^{(1)}(\kappa_2 r_{N-1})] = 0,\\
&H_{zN} = C_{N-1} J_0(\kappa_1 r_N) + D_{N-1} H_0^{(1)}(\kappa_1 r_N) = 0.
\end{aligned}
$$

Equations (22) can be solved in real quantities (in this case, $\mathrm{Im}\beta \approx 0$) and the first of them, for the known r_1, gives

$$
\mathrm{Re}\bar{n} \approx \left[n_0^2 - \left(\frac{\delta_1 \lambda_0}{2\pi r_1} \right)^2 \right]^{1/2}, \qquad (23)
$$

where $\delta_1 = 3.83171$ is the first nonzero root of the function $J_1(x)$.

According to (12) and (18), coefficients C_1 and D_1 in the second relation in (22) are

$$
C_1 = -\frac{1}{2}\mathrm{i}\pi\kappa_1 r_1 m_{11} C_0, \quad D_1 = -\frac{1}{2}\mathrm{i}\pi\kappa_1 r_1 m_{21} C_0,
$$

where m_{11} and m_{12} are defined by expressions (19).

By substituting the expressions for C_1, D_1, and $\mathrm{Re}\bar{n}$ in the condition $H_{z2} = 0$, we obtain the equation for r_2 in the form

$$
J_0(\kappa_1 r_2) N_1(\kappa_1 r_1) - J_1(\kappa_1 r_1) N_0(\kappa_1 r_2) = 0. \qquad (24)
$$

Similarly, from the relation for $E_{\varphi 3}$ in (22) we obtain the equation

$$
J_1(\kappa_2 r_3) N_0(\kappa_2 r_2) - J_0(\kappa_2 r_2) N_1(\kappa_2 r_3) = 0, \qquad (24a)
$$

from which r_3 can be determined from already known $\mathrm{Re}\bar{n}$ and r_2, etc.

By solving successively equations (22), the 'starting' values of variables required for the genetic algorithm are found. From a set of solutions with increasing values of each of the equations of type (24) and (24a), we choose the value of the desired coordinate that is closest to the required value corresponding to the particular optical thickness of the cladding layer (for example, the quarter-wavelength one or more).

In the large argument approximation, we can use the asymptotic form of cylindrical functions [47]. In this case, Eqn (24), for example, proves to be equivalent to the equation $\sin[\kappa_1(r_2 - r_1) + \pi/2] = 0$. It follows from this that $r_2 = r_1 + \pi(2p-1)/(2\kappa_1)$. By using (23), we obtain

$$
\kappa_1 = \frac{2\pi}{\lambda_0}\left[n_1^2 - n_0^2 + \left(\frac{\delta_1 \lambda_0}{2\pi r_1} \right)^2 \right]^{1/2}, \qquad (25)
$$

As a result, we have

$$
r_2 = r_1 + \frac{(2p-1)\lambda_0}{4} \times \left[n_1^2 - n_0^2 + \left(\frac{\delta_1 \lambda_0}{2\pi r_1} \right)^2 \right]^{-1/2}, \quad p = 1, 2, 3, \ldots . \qquad (26)
$$

Note that the same expression (26) is obtained by using the well-known result [12], which is the condition of the maximum reflection of light from a plane–parallel plate of thickness h ($h = r_i - r_{i-1}$),

$$
h = \frac{(2p-1)\lambda_0}{4n\cos\theta},
$$

where θ is the angle between the wave vector in a layer and the normal to its boundary, and n is the refractive index of the layer material. In particular, for the cladding layer

closest to the fibre core, we have $n = n_1$ in the latter relation and $\cos\theta = \{1 - (n_0/n_1)^2 + [\delta_1\lambda_0/(2\pi n_1 r_1)]^2\}^{1/2}$.

Recall, however, that expression (26) is approximate and corresponds (as in [12]) to a planar geometry (asymptotics of cylindrical functions).

One can see that the thickness of the first layer of the cladding in asymptotics is approximately proportional to an odd number of $\lambda_0/4$ (this result is approximate due to the presence of the third, generally speaking, small term in brackets). In this case, depending on the refractive-index contrast, the proportionality coefficient can be noticeably greater than unity, i.e. the real thickness of layers can exceed by several times $\lambda/4$ in vacuum, which is important for practical realisation of quarter-wavelength structures.

A similar dependence also takes place for optically less dense layers. In particular, to obtain the approximate value of r_3 in (24a), it is simply necessary to make the replacements $r_2 \to r_3$, $r_1 \to r_2$, and $n_1 \to n_2$ in (26).

The method for determining initial values of $\mathrm{Re}\bar{n}$ and r_i described above is most efficient and allows one to obtain the values of variables that are very close to real ones. The genetic algorithm further 'corrects' these values and finds their set providing, together with the required minimal $\mathrm{Im}\bar{n}$, the global minimum of $S_r(r_N)$ and satisfying equation (20).

To determine other radiation modes in a fibre optimised for the TE_{01} mode, the found geometry of the fibre is fixed. Then, the next root of Eqn (2) closest to the value of β for the TE_{01} mode will define the TE_{02} mode (this root has a greater value of $\mathrm{Im}\beta$ than the first root), the root following after the second root (with greater $\mathrm{Im}\beta$) will define the TE_{03} mode, etc. It is clear that this sequence of roots should be found from the dispersion equation only without using the genetic algorithm.

By using the dispersion equation for the TM modes in the same fibre optimised to the TE_{01} mode, all the sequence of the complex propagation constants of the TM_{0n} modes can be also determined. Similarly, by replacing Eqn (20) by dispersion equation (13), hybrid modes can be found. In this paper, we performed some calculations only for the lowest hybrid modes with the azimuthal parameter $m = 1$.

However, the optimisation of the structure of a BF with a glass core is somewhat complicated because the fundamental mode in such BFs is not the TE_{01} mode but the doubly degenerate lowest hybrid HE_{11} mode (see below). The start values of variables for optimisation are found here also from the condition that the radial component of the Poynting vector vanishes at all the interfaces in the layered cladding. In particular, in the same approximation $\mathrm{Im}\beta = 0$, the equality $S_r(r = r_1) = 0$ and the independence of S_r of the azimuthal angle φ for all r specify the relation between amplitudes in expressions for the field components, for example, in (12) and also allow one to determine $\mathrm{Re}\bar{n}$ from the equation

$$J_0(\kappa_0 r_1) = \frac{J_1(\kappa_0 r_1)}{\kappa_0 r_1}\left(1 - \frac{\mathrm{Re}\bar{n}}{n_0}\right), \tag{27}$$

where

$$\kappa_0 = \frac{2\pi n_0}{\lambda_0}\left[1 - \left(\frac{\mathrm{Re}\bar{n}}{n_0}\right)^2\right]^{1/2}.$$

It is easy to see that this equation can be quite accurately replaced by the equation $J_0(\kappa_0 r_1) \cong 0$ because, as a rule, $\mathrm{Re}\bar{n}/n_0 \approx 1$ and $|J_1(\kappa_0 r_1)/(\kappa_0 r_1)| < 1$.

Unlike (24) and (24a), the equations for determining coordinates of layer interfaces in the cladding, which also follow from equations $S_r(r = r_i) = 0$ $(i = 2, 3, ..., N)$ have a more complicated form. However, in the approximation of low-contrast refractive indices in cladding layers, these equations are reduced to expressions of type (24), (24a), and at the large arguments of cylindrical functions – to (26). In particular, the equation for determining r_2 has the form

$$J_1(\kappa_1 r_2)N_0(\kappa_1 r_1) - J_0(\kappa_1 r_1)N_1(\kappa_1 r_2) \approx 0. \tag{28}$$

Note that the procedure somewhat similar to the approximate method for determining the fibre structure geometry described above was applied in paper [19] where the authors determined the thickness of cladding layers by dividing intervals between the neighbouring roots of functions $J_0(x)$ and $J_1(x)$ by the values of the transverse wave number κ_j corresponding to the given layer. Note, however, that such an approach cannot be used to optimise BFs for the TE or TM modes.

After the consideration of various methods for optimising BFs with hollow and glass cores, it is pertinent to discuss in more detail the question of which of the BF modes is fundamental.

According to the definition of the fundamental mode as a mode with the lowest optical losses in a given fibre, either the TE_{01} or HE_{11} mode can be the fundamental mode in a BF. Let us present some relevant arguments.

On the one hand, it follows from (23) and (27), for example, that for any BF structure with a fixed r_1, the HE_{11} mode has the greatest real part of the propagation constant among all the modes. Indeed, from approximate equation (27) $[J_0(\kappa_0 r_1) \approx 0]$, we have with good accuracy

$$\mathrm{Re}\bar{n}_{HE} \approx \left[n_0^2 - \left(\frac{\delta_2\lambda_0}{2\pi r_1}\right)^2\right]^{1/2}, \tag{29}$$

where $\delta_2 = 2.40483$ is the first root of the function $J_0(x)$. By comparing (23) with (29), we see that $\mathrm{Re}\bar{n}_{HE} > \mathrm{Re}\bar{n}_{\mathrm{TE}}$. It also follows from this that the transverse component of the wave vector of the HE_{11} mode is the smallest, while the angle of its incidence on the core–cladding interface is the largest of all the angles of incidence of the guided modes in the fibre.

On the other hand, the dependence of the Fresnel coefficient R^2 of light power reflection from the plane interface between different media on the incident radiation polarisation is well known [12]. Indeed, if the electric vector of a wave is perpendicular to its plane of incidence, the dependence of R^2 on the angle of incidence θ has the form of a monotonically increasing (up to unity) function. But if the electric vector of the wave is parallel to the plane of incidence, the function $R^2(\theta)$, which also increases up to unity, is nonmonotonic and passes through the zero minimum at the Brewster angle. As a result, although both these dependences begin at the same point (for $\theta = 0$) and terminate at the same point (for $\theta = \pi/2$), the reflection coefficient is everywhere higher for the first polarisation than for the second one (except the two extreme points).

To use the result from [12], we will assume with good approximation that the TE_{01} or HE_{11} modes are plane waves and the core–cladding interface is a plane. Note also that the fields of TE modes have only the azimuthal electric

component, which is perpendicular to the plane of incidence of light on the first cladding layer, and therefore are not subjected to the Brewster effect. However, the HE_{11} mode field consists of two fields with orthogonal polarisations, and the second of these components (parallel) should be reflected weaker than the first one. Despite the grazing incidence of the HE_{11} mode, the presence of this radiation component reduces the total Fresnel reflection of the HE_{11} mode from the cladding, so that the TE_{01} mode proves to be the fundamental mode of the fibre. The general polarisation properties of Fresnel reflection mentioned above depend considerably on the contrast between refractive indices of the core and the first cladding layer. For comparatively high contrasts (for example, for hollow BFs), the dependences of the reflection coefficient on the angle of incidence for two polarisations noticeably differ (Fig. 1a), and the TE_{01} mode is reflected most strongly from the cladding, being the fundamental mode in this case. The HE_{11} mode, in which a part of energy corresponds to polarisation parallel to the plane of incidence, is reflected worse as a whole and to a great extent is refracted to the cladding.

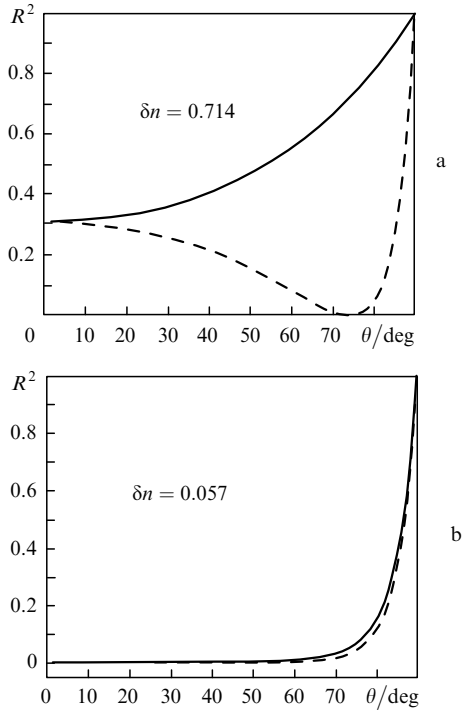

Figure 1. Dependences of the power coefficient of reflection from the interface of two media on the angel of incidence of light polarised in the plane of incidence (dashed curves) and in a plane perpendicular to the plane of incidence (solid curves). The contrast of the refractive indices of the media is $\delta n = (n_1 - n_2)/n_1$ $(n_1 > n_2)$.

If the contrast of refractive indices of the fibre core and cladding is small ($\Delta n \leqslant 0.1$), the influence of polarisation effects is considerably reduced and dependences of the reflectance on the angle of incidence for both polarisations become close, having small values of R^2 up to angles $\sim 70^\circ$ (Fig. 1b). In this case, the advantages of the TE_{01} mode over the HE_{11} mode are lost to a great extent.

The analysis performed above, which was based on the consideration of interaction of light with only one interface, is, of course, approximate, however, it comparatively simply explains the essence of the phenomenon. To obtain the quantitative relation between losses for the TE_{01} and HE_{11} modes at a low refractive-index contrast, it is necessary, of course, to take into account all other interfaces between cladding layers. Here, it is probably important that the angle of incidence of the HE_{11} mode (which is the fundamental mode in this case) on the layered structure is the greatest. In this case, losses for the TE_{01} mode can be comparable with those for the HE_{11} mode.

In a BF with a large core radius, when the arguments of cylindrical functions in the cladding are large, the period of a photonic crystal (the sum of thicknesses of two adjacent layers) in the entire cladding becomes approximately the same, and the optimisation of such BFs is reduced to the determination of the optimal values of the period and the thickness of layers in them. This does not mean, however, that the number of variables in the optimisation procedure noticeably decreases. Indeed, each additional layer in the cladding causes the redistribution of the field in the fibre and the corresponding change in the optimal geometry of the entire structure. It is obvious that the period changes with increasing N the stronger the lower the value of N itself. In other words, for large N, when the field behind the layered cladding becomes small, both the period and $\mathrm{Re}\bar{n}$ virtually become independent of N. As a result, the dependence $\mathrm{Re}\bar{n}(N)$ has the form of a function saturating with increasing N. Waveguide losses continue to decrease with increasing N.

If necessary, the approach described above can be used to optimise the BF structure for any mode. However, it is not obvious that this mode will 'survive' upon excitation of such a BF. It is most likely that some modes will propagate in the fibre with lower losses.

By changing the wavelength to both sides of λ_0 for any of the radiation modes at a fixed geometry, the dependences $\mathrm{Re}\beta(\lambda)$ and $\mathrm{Im}\beta(\lambda)$ are determined. The mode dispersion is found from the first of them. Calculations in the complex plane allow us to take into account both material losses (by introducing the imaginary parts depending on λ to expressions for the refractive indices n_0, n_1, and n_2 of the structure) and the material dispersion by assuming that the real parts of n_0, n_1, and n_2 depend on λ. Optical losses γ are defined as losses of the radiation intensity, i.e. $\gamma = 2\mathrm{Im}\beta = (4\pi\mathrm{Im}\bar{n})/\lambda$. Thus, losses in the units of dB km^{-1} can be found from the known relation (see, for example, [48])

$$\gamma = \frac{4 \times 10^{10} \pi \lg \mathrm{e}}{\lambda} \mathrm{Im}\bar{n}, \tag{30}$$

where λ is expressed in μm. One can see from (30) that, for example, to losses ~ 1 dB km^{-1} at $\lambda = 1.5$ μm, very low values of $\mathrm{Im}\bar{n}$ correspond ($\sim 3 \times 10^{-11}$). This justifies with a great margin the applicability of the approximation $\mathrm{Re}\bar{n} \gg \mathrm{Im}\bar{n}$ used everywhere.

Note that the radial distributions of the field components for modes in a BF are presented below in the normalised form. In the case of hybrid modes, the relation between A_0 and C_0 required for normalisation is presented below.

3. Results of calculations and discussion

The optical properties of guided radiation in BFs are analysed in the literature based on the geometry of the

multilayer fibre cladding used in each of the studies. The thickness of cladding layers is, as a rule, close to the quarter-wavelength one and is estimated by assuming the grazing incidence of light on the core–cladding interface. In this approximation, the relation between the thickness h_1 of denser layers and the thickness h_2 of less dense layers has the form (see, for example, [21])

$$\frac{h_1}{h_2} = \left(\frac{n_2^2 - 1}{n_1^2 - 1}\right)^{1/2}. \tag{31}$$

The geometrical parameters of a BF can be determined more accurately by solving equations of type (22). We will show below that the deviations of the layer thickness from the quarter-wavelength one appearing due to approximations can sometimes noticeably affect optical losses in BFs.

We will illustrate the results of optimisation of the BF geometry by comparing them with the data known from the literature. The optical properties of a BF with a hollow core of a large radius and a large refractive-index contrast in periodic layers of the cladding were calculated in [21]. The fibre parameters were $N = 17$, $\lambda_0 = 1.55$ μm, $r_1 = 13.02$ μm, $h_1 = 0.09444$ μm ($n_1 = 4.6$), and $h_2 = 0.33956$ μm ($n_2 = 1.6$). The minimal waveguide losses calculated for the TE_{01} mode in this fibre were $\sim 6\times\ 10^{-4}$ dB km^{-1} (this minimal value should correspond to the wavelength λ_0, whereas in [21] it corresponds for unknown reason to $\lambda \approx 1.66$ μm). By using the same initial values of r_1, n_1, n_2, N and λ_0 as in [21] and optimising the cladding structure geometry, we obtained $h_1 = 0.086375$ μm and $h_2 = 0.3085$ μm and minimal losses $\sim 2.9\times\ 10^{-4}$ dB km^{-1} at $\lambda_0 = 1.55$ μm. This example convincingly demonstrates a strong dependence of waveguide losses on the periodic cladding structure geometry – the change in the layer thickness only by 10 % reduces losses more than by half.

Note that waveguide losses characterise the degree of localisation of radiation guided in the fibre core. In the given case, waveguide losses are very small and the degree of light localisation is so high that material losses in cladding layers can be neglected with high accuracy.

There also exist papers in which the geometry of a multilayer cladding is very close to optimal; however, as a rule, the authors do not substantiate the choice of this geometry. For example, the parameters of a hollow BF in [27] were $N = 32$, $\lambda_0 = 1$ μm, $r_1 = 1.3278$ μm, $h_1 = 0.2133$ μm ($n_1 = 1.49$) and $h_2 = 0.346$ μm ($n_2 = 1.17$). For the TE_{01} mode in this fibre, the authors calculated $\bar{n} = 0.891067 + \mathrm{i}\cdot 1.4226 \times 10^{-8}$ ($\gamma = 776.4$ dB km^{-1}), whereas for the geometry optimised by us ($h_1 = 0.2146$, $h_2 = 0.3241$ μm) for the same parameters, we obtained $\gamma = 600$ dB km^{-1} for this mode (i.e. losses were smaller only by ~ 30 %). A similar result was obtained for another variant of the fibre with $r_1 = 1.8278$ μm calculated in [27] (other parameters were the same). In this case, the difference between optimised and non-optimised losses for the TE_{01} mode was also small (~ 32 %). The found values of $\mathrm{Re}\bar{n}$, as expected, coincided with good accuracy with the values calculated by expression (23).

Note also that calculations in [27] were performed by using the above-mentioned model [45]. If we calculate $\bar{n}$ for the periodic structure geometry used in [27] without the optimisation procedure, the results will exactly coincide with those obtained in [27]. This confirms the expressed assumption about the equivalence of our method for the calculation of the BF modes by using 4×4 matrices and the 2×2 matrix method applied in [45].

As another example we compare our results with calculations [30] of the lowest modes and their losses in a hollow BF with a cladding consisting of four pairs ($N = 8$) of layers made of Si ($n_1 = 3.5$) and Si_3N_4 ($n_2 = 2.0$). The authors of [30] calculated optical losses in the wavelength range from 1.5 to 1.7 μm in a BF fibre with the core radius $r_1 = 7.5$ μm and cladding layer thicknesses $h_1 = 0.11$ μm and $h_2 = 0.21$ μm. By optimising the geometry of this fibre, we obtained $h_1 = 0.1157$ μm and $h_2 = 0.235$ μm by assuming that $\lambda_0 = 1.7$ μm. This wavelength corresponds to the minimum of losses $\gamma \approx 0.62$ dB cm^{-1} in the dependence presented in [30]. Our calculations give $\gamma(\lambda_0) \approx 0.57$ dB cm^{-1}.

So far we considered fibres with claddings made of quarter-wavelength dielectric layers or having a similar structure. Such BFs have a transmission band with two bands with very large losses located on each side of it. The width of the long-wavelength band is infinite, whereas the short-wavelength band has a finite spectral width. In such fibres optimised to the specified wavelength λ_0, radiation at $\lambda > \lambda_0$ cannot propagate, and transmission bands exist only at shorter wavelengths. In the terminology of photonic crystals, transmission bands of BFs correspond to the so-called photon-forbidden bands in which light cannot propagate across the periodic structure of a photonic crystal and propagates only over its defects (in our case, a defect is the BF core). A photonic crystal is transparent in other spectral ranges, light is not reflected from the cladding and is not localised in the core, corresponding to BF bands with large losses.

In the short-wavelength spectral region, where the conditions $r_1 > \lambda$ and $h = h_1 + h_2 > \lambda$ are fulfilled, new properties of BFs are manifested, which are not typical for quarter-wavelength structures. Planar waveguides with a large cladding period proposed earlier [49–51] were called an ARROW (anti-resonant reflecting optical waveguide). They differ from waveguides with a quarter-wavelength layer cladding by a weak dependence of the spectral position of maxima of waveguide losses on h down to the radiation wavelength $\lambda \approx h$. As a whole it is assumed that the spectral parameters of an ARROW are mainly determined by the parameters of a layer closest to the core with a large refractive index (by its thickness and the refractive-index contrast in layers).

The properties of ARROWs are explained by the fact that the structure layers can be compared with Fabry–Perot (FP) resonators (or their cylindrical analogue). Indeed, it is clear from physical considerations that if the fibre cladding has spectral regions resonant with the given radiation wavelength, the radiation will be distributed in the fibre cross section so that its great fraction will be localised in these resonance regions. As a result, the resonance spectral bands (modes) of the FP cladding correspond to a weak transmission of light in the fibre because the redistribution of the radiation field due to its localisation in resonance regions reduces the radiation intensity in the core. And vice versa, the absence of resonances in the cladding corresponds to the spectral bands with the maximum transmission (hence the name ARROW for waveguides of this type). Physically, the resonance bands are related to a standing wave in a FP resonator.

In the general case the transmission spectrum of an ARROW should be determined by the resonance properties of optically denser and less dense cladding layers. Moreover, natural resonances (modes) are inherent both in a cladding period representing a complex FP resonator, which contains two dielectric media, and in a combination of many closely spaced layers. The number of possible resonators rapidly increases with increasing N. The discrete eigenfrequencies (modes) of each complex resonator do not coincide in the general case with frequencies for individual layers and frequencies of other resonators. Therefore, the cladding can have a considerable number of resonance frequencies in a particular spectral range. The resonance frequencies of individual layers can be easily estimated analytically, whereas the determination of the eigenfrequencies of multi-layer resonators is a more complicated problem, which is beyond the scope of our paper.

Thus, the quarter-wavelength structure of the cladding corresponds to the absence of FP resonances when the ARROW transmission is maximal. If the thickness of layers is a multiple of even numbers of a quarter of the wavelength (of integers of half-waves), the conditions of FP resonances are realised, and an ARROW with such a structure does not virtually transmit radiation. The intermediate values of layer thicknesses correspond to intermediate regions between bands with high and low ARROW losses.

Radiation mode losses rapidly decrease with increasing the number of layer periods, but, as mentioned above, the addition of these new periods does not change the spectral position of maxima of losses in fibres if $h > \lambda$.

The properties of planar ARROWs considered above are also inherent in cylindrical waveguides, which were studied in a number of papers (see, for example, [25, 26, 31]). The theoretical analysis of BFs of the ARROW type does not differ in principle from our analysis presented above. Therefore, we will not consider them as a separate class of BFs, but simply will illustrate their properties by a number of examples.

Thus, Fig. 2 presents the transmission spectrum of an ARROW with arbitrarily chosen parameters. Resonance conditions for an optically dense layer (with n_1) have the form $\kappa_1 h_1 = \pi q$ (here, $q = 1, 2, 3$) is an integer of radiation half-wavelength fitting in the resonator length h_1. By using (25), we find for the TE modes the approximate resonance wavelengths in optically dense cladding layers

$$\lambda_{1,q} = \frac{2h_1(n_1^2 - n_0^2)^{1/2}}{[q^2 - (\delta_1 h_1/\pi r_1)^2]^{1/2}}. \qquad (32)$$

The wavelengths $\lambda_{1,q}^{(a)}$corresponding to the absence of resonances in these layers (anti-resonance) are also well described by (32) with the replacement $q \to q + 1/2$.

One can see from Fig. 2 that the spectrum has several forbidden bands (bands with small losses) even within a range of moderate width and all the resonances determined from (32) fall into ARROW bands with the smallest transmission. Note at the same time that not all anti-resonances of the first cladding layer determined by (32) correspond to photon-forbidden bands. Thus, according to Fig. 2, the loss level at wavelengths $\lambda_{1,8}^{(a)} = 1.583$, $\lambda_{1,9}^{(a)} = 1.415$, $\lambda_{1,11}^{(a)} = 1.168$, and $\lambda_{1,12}^{(a)} = 1.075$ μm corresponding to anti-resonances in (32) with $q = 8$, 9, 11, 12 is $2\times10^4 - 5\times 10^5$ dB km^{-1}, whereas these losses at other resonances ($q = 7$, 10, 13 at $\lambda_{1,7}^{(a)} = 1.795, \lambda_{1,10}^{(a)} = 1.28$, $\lambda_{1,13}^{(a)} = 0.995$ μm) are 6–7 orders of magnitude lower. Such a difference can be explained only by the fact that at wavelengths close to anti-resonances with $q = 8$, 9, 11, and 12 there exist resonances (cladding modes) in other, more complex resonators, which were mentioned above. The interaction of these cladding modes with the anti-resonances of the first layer leads, as a rule, to the spectral shift of the low-loss bands with respect to its position predicted by expression (32). For example, the expected loss minimum at $\lambda_{1,8}^{(a)} = 1.583$ μm appears at a wavelength of 1.625 μm. A similar behaviour is observed for anti-resonances at $q = 9$, 11, 12. As a result, not all the optical properties of an ARROW are found to be determined by the parameters of only one first layer.

The FP resonances of optically less dense ARROW layers (with n_2) can affect the width of bands with large losses. Indeed, the positions of these additional resonances, similarly to (32), can be found from the expression

$$\lambda_{2,p} = \frac{2h_2(n_2^2 - n_0^2)^{1/2}}{[p^2 - (\delta_1 h_2/\pi r_1)^2]^{1/2}}, \quad p = 1, 2, 3, \ldots . \qquad (33)$$

One can see from (33) and Fig. 2 that the resonance wavelengths $\lambda_{2,p}$ for the given particular parameters of the fibre are close to the corresponding $\lambda_{1,q}$ and fall into the same minimal transmission ARROW bands. But even all resonances (32) and (33) cannot completely explain the calculated spectrum. Spectral bands with high losses should be determined by some other resonances (modes) which can be caused, for example, by the presence of more complex resonances in the structure, which were neglected in the model.

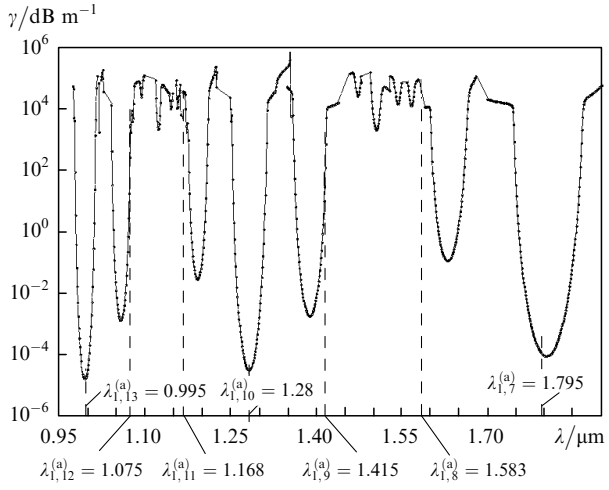

Figure 2. Calculated transmission spectrum for the TE_{01} mode in an ARROW; $n_0 = 1$, $n_1 = 3.5$, $n_2 = 1.5$, $h_1 = h_2 = 2$ μm, $r_1 = 4$ μm, $N = 20$, the values of $\lambda_{1,q}^{(a)}$ are in μm.

Because the analysis of the spectrum as a whole in Fig. 2 is quite complicated, we consider one of the anti-resonance bands (photon-forbidden bands) with minimal losses at $\lambda_{1,10}^{(a)} = 1.28$ μm at the enlarged wavelength scale (Fig. 3). The shape of this curve is typical for the wavelength dependence of the TE_{01} mode losses in BFs. The ARROW properties are discussed below by the example of this forbidden band.

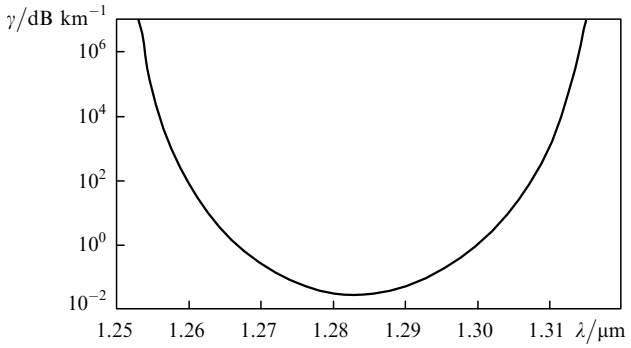

Figure 3. Photon-forbidden band in an ARROW with minimal losses at $\lambda_{1,10}^{(a)} = 1.28$ μm (see Fig. 2).

Figure 4 presents the radial distributions of one of the two field components (H_z) determining the radial energy flux (waveguide losses) S_r in a hollow ARROW. The distributions are presented at the points of the spectrum (see Fig. 2) with minimal losses in the photon-forbidden band shown in Fig. 3 and at one of the points in the high-loss band adjacent to this band. One can see from Fig. 4a that in the 'anti-resonance' case, neither of the cladding layers contains an integer of radiation half-wavelengths. However, despite comparatively low losses in the fibre, the field amplitudes in layers closest to the fibre core are large

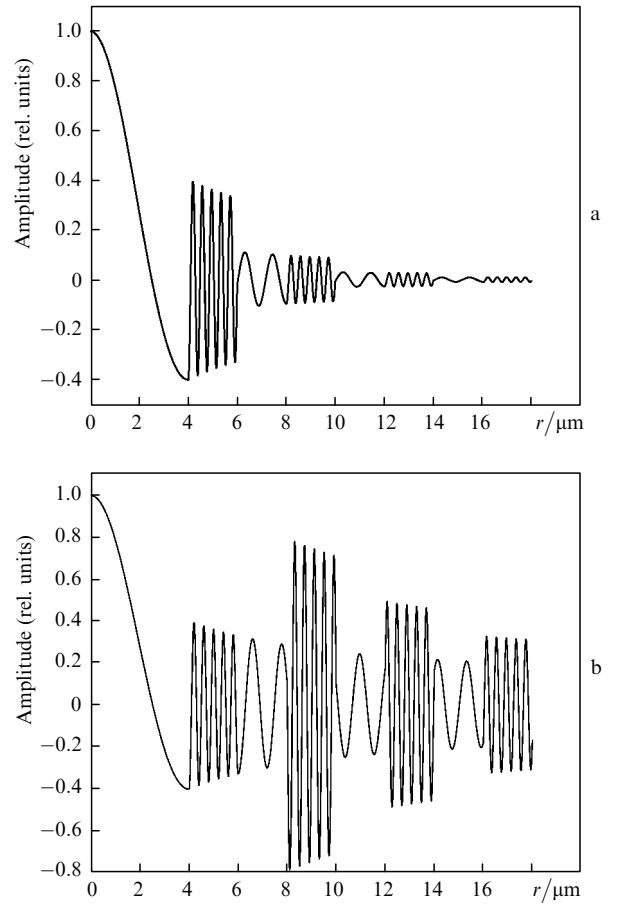

Figure 4. Radial distributions of H_z normalised to the maximum for the minimal losses in an ARROW at $\lambda_{1,10}^{(a)} = 1.28$ μm (a) and for large losses at $\lambda_{1,10} = 1.344$ μm (b) (see Fig. 2).

enough. This can indicate that although the cladding geometry, which we have chosen arbitrarily, gives minimal losses at a wavelength of 1.28 μm, it does not exactly correspond to the quarter-wavelength structure for this wavelength and can be in principle optimised. The optimisation should reduce the field amplitude in the cladding and losses. The latter assumption is confirmed by calculations from which it follows that the decrease in the thickness of cladding layers down to the optimal value 1.976 μm reduces losses at least by a factor of one and a half.

The radial distribution of the second field component E_φ determining S_r exhibits a similar behaviour.

The field distribution for the resonance wavelength $\lambda_{1,10} = 1.344$ μm presented in Fig. 4b shows that the field is indeed concentrated to a great extent in cladding layers. In this case, the thickness of each optically dense layer fits ten half-wavelengths, as should be in the resonance case. One can also see that layers with the smaller refractive index n_2 do not contain an integer of half-wavelengths and resonances are absent, which follows, by the way, from (33). Note, however, that the field amplitudes decrease non-monotonically both in optically denser and less optically dense layers. In our opinion, this is explained by the fact that each of the layers, being an independent FP resonator, also serves as a component of a number of complex resonators consisting of several successive layers. Because the eigenfrequencies of such numerous resonators are different, the total contribution of these frequencies to the resonance response of each cladding layer to the given radiation wavelength is also different.

We see that there exist a number of spectral properties of ARROWs that can be explained only by considering the influence of composite resonators forming the cladding. Their substantial role is indirectly confirmed in paper [44] where it was shown that the resonance properties of a new layer added to the cladding structure (although with parameters different from those of regular cladding layers) considerably changed the ARROW spectrum.

Microstructure fibres of different types, in which instead of coaxial cladding layers with a high refractive index n_1 the cylindrical rods of radius $R > \lambda$ with the same refractive index n_1 are located around the optically less dense core, have spectral properties similar to those of ARROWs. The positions of resonance spectral bands in such structures are related to the cut-off wavelengths of the eigenmodes of the rods in the cladding photonic crystal [52–57].

As for the group velocity dispersion in BFs, by assuming that the material dispersion is absent, we are dealing with the waveguide dispersion only. This dispersion is completely determined by the properties of a particular photon-forbidden band. The dispersion parameter is defined as

$$D = -\frac{2\pi c}{\lambda^2}\frac{\mathrm{d}^2 \mathrm{Re}\beta}{\mathrm{d}\omega^2} = -\frac{\lambda}{c}\frac{\mathrm{d}^2 \mathrm{Re}\bar{n}}{\mathrm{d}\lambda^2}, \tag{34}$$

i.e. the photon-forbidden band is characterised by the dependence $\mathrm{Re}\bar{n}(\lambda)$.

The effective mode refractive index for the photon-forbidden band under study (see Fig. 3) is presented in Fig. 5. The straight dashed lines show the boundaries of the photon-forbidden band. The strong interaction of modes in the fibre core with cladding modes (resonances of all possible FP resonators in the cladding) leads to numerous

'anti-crossings' of the dispersion curves of interacting modes, one of which is shown near a wavelength of 1.25 μm. The boundaries of the photon-forbidden band are determined by the loci of the anti-crossings. A similar dependence for the HE_{11} mode is located somewhat higher than the dependence shown in Fig. 5 (but, of course, lower than the unit level), while the dependence for the TE_{02} mode is located lower. However, these modes have considerably higher optical losses than the TE_{01} mode, and we will not discuss them here.

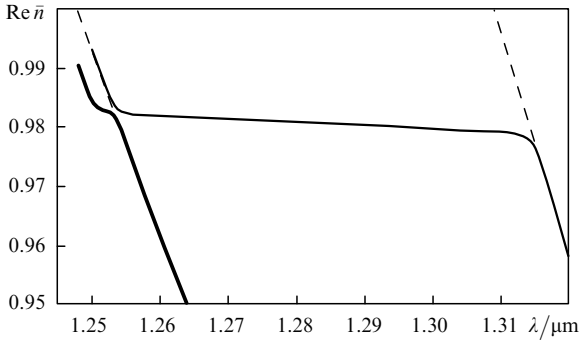

Figure 5. Wavelength dependence of the real part of the effective mode refractive index in the photon-forbidden band in Fig. 3 (the TE_{01} mode). The boundaries of the photon-forbidden band are shown by dashed straight lines.

The mode dispersion $D(\lambda)$ calculated from (34) by using the function $\mathrm{Re}\bar{n}(\lambda)$ in Fig. 5 is presented in Fig. 6. This dependence is also typical for BFs and is characterised by very large absolute values of dispersion near the boundaries of the photon-forbidden band, but unfortunately they are characterised by very large optical losses. At the same time, dispersion values in the region of acceptable losses are still large, as the inset in Fig. 6 shows. This property of BFs can be used to control dispersion in various optical devices.

Recall now that we calculated the dependence $\mathrm{Re}\bar{n}(\lambda)$ by neglecting the material dispersion. In the spectral region where hollow BFs have low optical losses, the wavelength dependence of the material refractive index can be neglected because the fraction of light propagating in the cladding material is quite small. At the same time, the spectral position of the zero dispersion in glass BFs can be found sufficiently accurately only by taking into account the material dispersion.

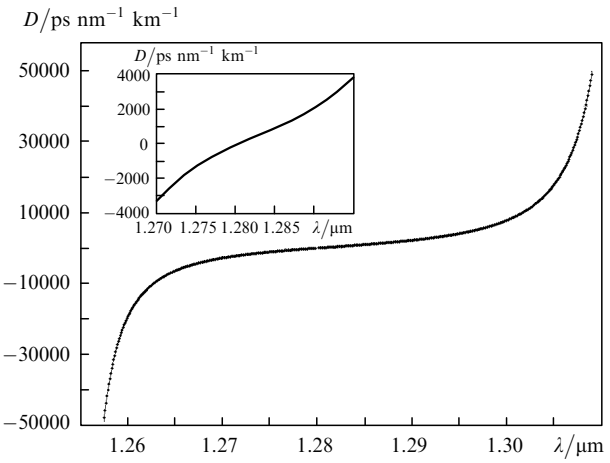

Figure 6. Dispersion parameter D calculated for the TE_{01} mode in the photon-forbidden band in Fig. 3.

4. Conclusions

We have considered in detail one of the most efficient methods for calculating the optical properties of Bragg optical fibres. The method can be used not only to find the mode composition of radiation, optical losses and dispersion in fibres with the specified geometry of a multilayer cladding but, in conjunction with the genetic algorithm, also to determine the optimal cladding structure providing minimal optical losses at a particular wavelength. It has been explained simply which of the modes should be fundamental in BFs with high and low contrasts between refractive indices of the fibre core and cladding. The possibility of using BFs as efficient mode filters is confirmed, especially, in the case of a high refractive-index contrast. Such BFs with a hollow cladding can have in principle very low optical losses for the fundamental TE_{01} mode. The basic properties of BFs of the ARROW type have been described and it has been shown that these properties are determined not only by the parameters of the cladding layer nearest to the core but also by resonances of the cladding as a whole and of layered resonators comprising the cladding. Interest in BFs of the ARROW type is caused by practical considerations because it is possible to fabricate fibres with comparatively broad transmission bands (a few tens of nanometres) with acceptable optical losses (see, for example, Fig. 3).

Note that, being potentially single-mode and guiding only one cylindrically symmetric and nondegenerate TE_{01} mode, hollow BFs are not subjected to the influence of the polarisation mode dispersion.

Acknowledgements. This work was supported by the Russian Foundation for Basic Research (Grant No. 07-02-01244).

References

1. Yeh P., Yariv A., Marom E. *J. Opt. Soc. Am.*, **68**, 1196 (1978).
2. Doran N.J., Blow K.J. *J. Lightwave Technol.*, **1**, 588 (1983).
3. Lazarchik A.N. *Radiotekh. Radioelektron.*, **33**, 36 (1988).
4. Martijn de Sterke C., Bassett I.M., Street A.G. *J. Appl. Phys.*, **76**, 680 (1994).
5. Xu Y., Lee R.K., Yariv A. *Opt. Lett.*, **25**, 1756 (2000); *OFC'2001* (Anaheim, 2001) Vol. 2, TuC7.
6. Melekhin V.N., Manenkov A.B. *Zh. Tekh. Fiz.*, **38**, 2113 (1968).
7. Melekhin V.N., Manenkov A.B., in *Elektronika bol'shikh moshchnostei* (High-power Electronics) (Moscow: Nauka, 1969) No. 6, p. 161.
8. Manenkov A.B. *Izv. Vyssh. Uchebn. Zaved., Ser. Radiofiz.*, **14**, 606 (1971).
9. Manenkov A.B. *Radiotekh. Radioelektron.*, **22**, 2043 (1977).
10. Manenkov A.B., Melekhin V.N. *Radiotekh. Radioelektron.*, **24**, 1282 (1979).
11. Nikolaev V.V., Sokolovskii G.S., Kalitievskii M.A. *Fiz. Tekh. Poluprovodn.*, **33**, 174 (1999).
12. Born M., Wolf E. *Principles of Optics* (Oxford: Pergamon Press, 1969; Moscow: Nauka, 1973).
13. Fink Y., Ripin D.J., Fan S., et al. *J. Lightwave Technol.*, **17**, 2039 (1999).

14. Brechet F., Roy P., Marcou J., Pagnoux D. *Electron. Lett.*, **36**, 514 (2000).
15. Brechet F., Leproux P., Roy P., Marcou J., et al. *Electron. Lett.*, **36**, 870 (2000).
16. Temelkuran B., Hart S.D., Benoit G., et al. *Nature*, **420**, 650 (2002).
17. Kawanishi T., Izutsu M. *Opt. Express*, **7**, 10 (2000).
18. Ibanescu M., Fink Y., Fan S., et al. *Science*, **289**, 415 (2000).
19. Marcou J., Brechet F., Roy P. *J. Opt. A: Pure Appl. Opt.*, **3**, S144 (2001).
20. Ouyang G., Xu Y., Yariv A. *Opt. Express*, **9**, 733 (2001).
21. Johnson S.J., Ibanescu M., Skorobogatiy M., et al. *Opt. Express*, **9**, 748 (2001).
22. Hart S.D., Maskaly G.R., Temelkuran B., et al. *Science*, **296**, 510 (2002).
23. Xu Y., Ouyang G., Lee R.K., Yariv A. *J. Lightwave Technol.*, **20**, 428 (2002).
24. Ouyang G., Xu Y., Yariv A. *Opt. Express*, **10**, 899 (2002).
25. Litchinitser N.M., Abeeluck A.K., Headley C., Eggleton B.J. *Opt. Lett.*, **27**, 1592 (2002).
26. Abeeluck A.K., Litchinitser N.M., Headley C., Eggleton B.J. *Opt. Express*, **10**, 1320 (2002).
27. Bassett I.M., Argyros A. *Opt. Express*, **10**, 1342 (2002).
28. Argyros A. *Opt. Express*, **10**, 1411 (2002).
29. Ibanescu M., Johnson S.G., Soljacic M., et al. *Phys. Rev. E*, **67**, 046608 (2003).
30. Xu Y., Yariv A., Fleming J.G., Lin S-Yu. *Opt. Express*, **11**, 1039 (2003).
31. Engeness T.G., Ibanescu M., Johnson S.G., et al. *Opt. Express*, **11**, 1175 (2003).
32. Litchinitser N.M., Dunn S.C., Usner B., et al. *Opt. Express*, **11**, 1243 (2003).
33. Fevrier S., Viale P., Gerome F., et al. *Electron. Lett.,* **39**, 1240 (2003).
34. Guo Sh., Albin S., Rogowski R.S. *Opt. Express*, **12**, 198 (2004).
35. Kuriki K., Shapira O., Hart S.D., et al. *Opt. Express*, **12**, 1510 (2004).
36. Yi Ni, Lei Z., Chong Gu, et al. *Opt. Express*, **12**, 4602 (2004).
37. Alam I., Sakai Jun-ichi. *Opt. Commun.*, **250**, 84 (2005).
38. Fevrier S., Jamier R., Blondy J.-M., et al. *Proc. ECOC 2005* (Glazgow, 2005) Vol. 6, Pap. Th4.4.3; *Opt. Express*, **14**, 562 (2006).
39. Ibrahim Abdel-Baset M.A., Choudhury P.K., Alias M.S. *Optik*, **117**, 33 (2006).
40. Likhachev M.E., Uspenskii Yu.A., Semenov S.L., et al. *Proc. ECOC 2005* (Glazgow, 2005) Vol. 6, Pap. Th4.2.5.
41. Likhachev M.E., Semenov S.L., Bubnov M.M., et al. *Kvantovaya Elektron.*, **36**, 581 (2006) [*Quantum Electrom.*, **36**, 581 (2006)].
42. Sakai Jun-ichi. *J. Opt. Soc. Am. B*, **22**, 2319 (2005).
43. Sakai Jun-ichi. *J. Opt. Soc. Am. B*, **24**, 9 (2007).
44. Uspenskii Yu.A., Likhachev M.E., Semenov S.L., et al. *Opt. Lett.*, **32**, 1202 (2007).
45. Chew W.C. *Waves and Fields in Inhomogeneous Media* (New York: Van Nostrand, 1990).
46. Goldberg D.E. *Genetic Algorithms in Search, Optimization and Machine Learning* (Boston, MA: Kluwer Acad. Publ., 1989).
47. Abramowitz M., Stegun I.A. (Eds) *Handbook of Mathematical Functions* (New York: Dover, 1965; Moscow: Nauka, 1979).
48. Poladian L., Issa N.A., Monro T.M. *Opt. Express*, **10**, 449 (2002).
49. Kokubun Y., Baba T., Sakaki T. *Electron. Lett.*, **22**, 892 (1986).
50. Baba T., Kokubun Y., Sakaki T., et al. *J. Lightwave Technol.*, **6**, 1440 (1988).
51. White T.P., McPhedran R.C., Martijn de Sterke C., et al. *Opt. Lett.*, **27**, 1977 (2002).
52. Laegsgaard J. *J. Opt. A: Pure Appl. Opt.*, **6**, 798 (2004).
53. Luan F., George A.K., Hedley T.D., et al. *Opt. Lett.*, **29**, 2369 (2004).
54. Argyros A., Birks T.A., Leon-Saval S.G., et al. *Opt. Express*, **13**, 309 (2005).
55. Bouwmans G., Bigot L., Quiquempois Y., et al. *Opt. Express*, **13**, 8452 (2005).
56. Roberts P.J., Couny F., Sabert H., et al. *Opt. Express*, **13**, 236 (2005).
57. Renversez G., Boyer P., Sagrini A. *Opt. Express,* **14**, 5682 (2006).